SELENIUM DOPING ENHANCES THE CONDUCTIVITY OF LIQUID PHASE SYNTHESISED Na_3PS_4 AS A SOLID ELECTROLYTE FOR All SOLID STATE SODIUM BATTERIES

Mohammed Hassan [1, 2], Raheed Bolia[1, 2], Dries De Sloovere[1, 2, 3], Jonas Mercken[1, 2, 3], Marlies Van Bael[1,2,3], An Hardy[1, 2, 3]

[1] Hasselt University, Institute for Materials Research (imo-imomec), Design and Synthesis of Inorganic Materials (DESINe), Martelarenlaan 42, B-3500 Hasselt, Belgium

[2] imec, imo-imomec, Wetenschapspark 1, B-3590 Diepenbeek, Belgium

[3] Energyville, imo-imomec, Thor Park 8320, B-3600 Genk, Belgium

Corresponding author: Mohammed Hassan (mohammed.saleh@uhasselt.be)

Abstract

A scalable, cost-effective liquid-phase synthesis method has shown promise for producing Na_3PS_4 sulfide-based solid electrolytes. However, the ionic conductivity of the resulting solid electrolyte has been insufficient for applications in all-solid state sodium batteries. In this work, solid electrolytes in which selenium (Se) partially substitutes phosphorus (P) in the series $Na_{3+x}P_{1-x}Se_xS_4$ ($0.000 \leq x \leq 0.150$) were successfully synthesized via the liquid-phase method. The newly synthesized solid electrolytes retained the cubic structure of the glass-ceramic and demonstrated ionic conductivity comparable to Na_3PS_4 prepared by the ball-milling method. The synthesized samples were effectively applied in all-solid-state sodium batteries containing a TiS_2-solid electrolyte composite as the cathode and $Na_{15}Sn_4$ as the anode, achieving an initial capacity of approximately 125 mA h g^{-1} based on the weight of the TiS_2

Keywords: Se substituted Na_3PS_4, Liquid phase method, All solid-state sodium battery.

1. Introduction

All-solid-state sodium batteries are being developed as safe and cost-effective energy storage technologies. A crucial component of these batteries is the solid electrolyte, often also functioning as the separator. Replacing liquid electrolytes with solid electrolytes can mitigate one of the major drawbacks of current liquid-based batteries: safety concerns due to the flammability of the liquid electrolyte [1]. Sulfide-based inorganic compounds, including thiophosphates, argyrodites, and their derivatives, represent one of the potential promising options for viable solid electrolytes. These inorganic materials are known for their high ionic conductivity and low-temperature processing [2].

While lithium batteries are now the widespread technology in energy storage applications, the scarcity of lithium, its geopolitical distribution, and the surge of demand cause a huge stress on its prices [3, 4]. It is, therefore, necessary to introduce another integrated/competitive battery chemistry to restore the balance to the market. Sodium-based batteries are potentially viable alternative options, as sodium ions greatly resemble lithium in their properties and, above of that has virtually unlimited resources on earth [5]. For a sulfide-based all-sodium solid-state battery, Na_3PS_4 and its derivatives, glass ceramics, represent the primary option. The pristine Na_3PS_4 is usually synthesised by the solid ball mill method and has an ionic conductivity near 0.1 mS cm^{-1}[6]. However, it was reported that the ball mill method is difficult to scale up for the synthesis of sulfides due to inhomogeneities and low product yield [7]. Further disadvantages of the ball mill method are the high mechanical energy consumption and the noise pollution accompanying the process [8]. For these reasons, researchers have turned their attention to the liquid phase method as a safe, high-yield, and affordable method [9, 10].

The use of the liquid phase method has previously succeeded in creating the required phases of many sulfide-based solid electrolytes. However, in most of these cases, the ionic conductivity of these phases is lower than their ball mill synthesized counterparts [11]. For example, Na_3PS_4 has been attempted to be synthesized by the liquid phase method using different solvents, resulting in glass ceramics with about one order of magnitude lower conductivity than the same phase synthesized by the ball mill method [12-14]. The low ionic conductivity of these solid electrolytes limits their application in all sodium solid-state batteries.

Doping can effectively improve the ionic conductivity of Na_3PS_4. The ultimate effect of the doping process on the properties of the host material was found to depend on the relative physicochemical characteristics of the dopant [15]. For instance, Na_3PS_4 doped with Cl, Si, Ca, and W has yielded glass-ceramics with enhanced ionic conductivity and improved properties such as chemical stability [16-19]. However, all previous attempts relied on ball milling, leaving it unclear if the same phases could be achieved through liquid-phase synthesis.

In this work, we investigated the substitution of phosphorus with selenium in Na_3PS_4, producing the $Na_{3+x}P_{1-x}Se_xS_4$ series via a liquid-phase synthesis route. This approach successfully yielded glass–ceramic electrolytes with ionic conductivities comparable to those of their ball-milled counterparts. The composition with the highest ionic conductivity demonstrated promising performance when implemented in an all-solid-state sodium battery.

2. Experimental

2.1. Materials and synthesis

Na_3PS_4 and Se-substituted Na_3PS_4 were synthesized via a liquid-phase method using Na_2S (95%, Thermo Scientific), P_2S_5 (99%, Sigma-Aldrich), and SeS_2 (>95%, Sigma-Aldrich) as starting materials. Anhydrous acetonitrile (99.8%, Sigma-Aldrich) was chosen as the solvent due to its previously reported effectiveness in producing Na_3PS_4 with relatively high ionic conductivity [20]. The starting materials were first hand-ground in stoichiometric proportions (for the series $Na_{3+x}P_{1-x}Se_xS_4$, with x ranging from 0.000 to 0.150) using an agate mortar and pestle. The ground mixture was then transferred to a glass vial, to which anhydrous acetonitrile was added at a ratio of 6 g solvent per 0.3 g of solid. This mixture was stirred magnetically at 600 rpm for 24 hours at 50° C, after which the solvent was removed by vacuum drying at room temperature using a Schlenk line. The resulting dry powder was then heated under vacuum at 270°C in an attached tube furnace (ThermoConcept) for 6 hours. Owing to the limited ionic conductivity of the liquid-phase-synthesized undoped Na_3PS_4, it could not serve as a benchmark solid electrolyte in the solid-state battery. Instead, a Na_3PS_4 sample prepared via ball mill is used for this purpose. This sample is referred to as ‘pristine’. The term ‘undoped’ is reserved for the Na_3PS_4 synthesized by the liquid phase method throughout the article.

The pristine sample was prepared by hand mixing the starting materials as before and then transferring them to a 40 ml zirconia ball mill jar with 6 zirconia balls (10 cm diameter) inside an argon glove box. The jars were sealed and taken out of the glove box to the ball mill (Retsch-Emax). The milling was conducted at 510 rpm for 5 hours, and the milled powder was subsequently heated under the same conditions as in the liquid-phase method.

A sample with the nominal composition $Na_{3.075}P_{0.925}Se_{0.075}S_4$ was analyzed by ICP-OES (Perkin Elmer Optima 3300 DV simultaneous spectrometer) for quantitative determination of selenium. A 10.83 mg portion was dissolved in 20 mL of 1 mol dm^{-3} NaOH, and the resulting solution was diluted 100-fold prior to measurement. The measured selenium content of 0.2956 mg was in close agreement with the calculated value of 0.2744 mg, indicating that the nominal stoichiometry was achieved. From this observation, indirectly it can be inferred that selenium may be incorporated at the phosphorus site.

The anode material $Na_{15}Sn_4$ was prepared following a modified procedure of Tanibata et al. [21]. Stoichiometric amounts of Na (foil) and Sn (powder) metals were added to a ball mill jar (45 ml) with 10 zirconia balls (10 mm diameter), and then ball milling was carried out at 510 rpm for 5 hrs. The cathode material was prepared by hand mixing of TiS_2 (Thermo Scientific, 200 Mesh, 99.8%) and the solid electrolyte in a 1:1 ratio, using an agate mortar and pestle. TiS_2-solid electrolyte composite provides better contact between the cathode and the solid electrolyte and improves the battery performance compared to TiS_2 alone [22].

All the above procedures were performed either in vacuum or in an argon-filled glove box (Sylatech) with humidity < 3 ppm and oxygen <1 ppm.

2.2. Structural characterizations

2.2.1. X-ray diffraction

The XRD diffractograms were obtained using a Bruker D8 with a Cu X-ray source. The samples were packed into glass capillary tubes of radius 1.5 mm, sealed inside the glove box, and sent for analysis.

2.2.2. Raman spectroscopy

Raman spectra of the samples were collected using a Renishaw InVia Qontor microscope within the 100-1000 cm^{-1} range, employing a 532 nm laser. Approximately 2 mg of the sample was deposited onto a glass substrate within the glovebox, sealed with a square cover glass using vacuum grease, and placed inside a plastic boiling tube. The boiling tube was then transferred from the glovebox to the Raman analysis chamber within a tightly closed stainless-steel canister.

2.2.3. Thermogravimetric analysis

TGA-DSC measurements were conducted using a TA-SDT Q600 V20.9 Build 20 instrument over a temperature range of room temperature to 300 °C, at a heating rate of 10 °C/min. To minimize exposure to air, the samples were weighed into a platinum pan inside an argon-filled glovebox. The pan was then kept in a glass vial and sealed, and then transferred to the TGA-DSC instrument. The vial was opened, and the sample was quickly transferred to the instrument's sample stage, followed by the immediate initiation of a nitrogen flow at 100 mL/min.

2.4. Electrical conductivity and electrochemical characterization

To evaluate ionic conductivity, pellets from the powders were pressed under 5 tonnes of mechanical pressure using an 8 mm die, resulting in thicknesses ranging from 0.6 to 1.1 mm. These pellets were sandwiched between two stainless steel electrodes connected to a potentiostat (Metrohm P6STAT302N). A mechanical pressure of 1000 kg was applied to the pellet during the measurements to improve the electrical contact. Impedance spectra were acquired within 0.5 MHz – 100 Hz frequency range at a 50-mV amplitude and then fitted to a suitable equivalent circuit using ZView software to determine ionic conductivity.

Electrochemical stability was assessed using cyclic voltammetry. A half-cell configuration was employed, comprising a sodium metal as reference electrode, a pelletized powder as solid electrolyte, and a stainless-steel working electrode. A Metrohm PGSTAT302N was used as a potentiostat. The voltage range was set to -0.5-4 V, with a scan rate of 1 mV/s.

All solid-state cell was assembled by distributing ca. 2 mg of the positive electrode (TiS_2-solid electrolyte composite) at the bottom of an 8 mm hard steel die. Next, approximately 50 mg of the solid electrolyte was added on top of the positive electrode and finally 20 mg of $Na_{15}Sn_4$. The three layers were pressed to a pressure of 5 tonnes and held under this pressure for 3 minutes. The resultant pellet was connected to stainless steel leads of a Swagelok cell, which was then sealed and locked tightly inside the glove box. The performance of cell was tested using Bio-Logic potentiostat in the voltage range 1-2.8 V. Two batteries were tested, one with $Na_{3.05}P_{0.95}Se_{0.05}S_4$ and the other with pristine ball milled Na_3PS_4 as solid electrolytes.

3. Results and Discussion

3.1. Structural characterization

3.1.1. X-ray diffraction

The XRD patterns of undoped and four selected Se-substituted Na_3PS_4 samples as prepared via the liquid phase method are shown in Figure 1. All peaks can be indexed in the cubic Na_3PS_4 phase, which is typically stable at high temperatures but has been stabilized by coexisting with its amorphous phase [6]. The cubic phase is accompanied by minor amounts of the tetragonal phase as evidenced by the peak at 38.5° that results from the diffraction line (212) [23]. However, this peak diminishes in the patterns of Se-substituted samples and nearly vanishes in those with high Se content, indicating an increase in the purity of the cubic phase. Additionally, unidentified relatively weak peaks are observed in the patterns of high Se content samples. Overall, the Se substituted Na_3PS_4 samples retained the pure cubic phase, which suggests the successful substitution of P with Se in the studied range.

The XRD patterns were analyzed by Rietveld refinement using the FullProf Suite 5.2, and the refined profiles are presented in Figure S1(a-e). The corresponding lattice parameters (*a*) are summarized in Table S1. For undoped Na_3PS_4, the refined value of *a* is 7.0025 ± 0.0004 Å. Upon partial substitution of P with Se, *a* increases slightly to 7.0168 ± 0.0002 Å in $Na_{3.075}P_{0.925}Se_{0.075}S_4$, and then remains nearly constant at this value for $Na_{3.15}P_{0.85}Se_{0.15}S_4$. This expansion is consistent with the observed shift of the diffraction peaks to lower angles, which can be attributed to the replacement of the smaller P^{5+} ions (0.25 Å) with larger Se^{4+} ions (0.37 Å) [24]. Beyond x = 0.075, the lattice parameter appears to saturate, indicating that no additional Se^{4+} ions can be effectively accommodated in the structure.

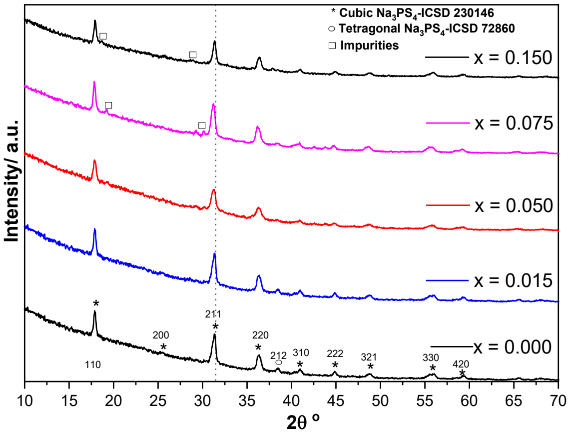

Figure 1. XRD patterns of $Na_{3+x}P_{1-x}Se_xS_4$, glass ceramics, x = 0- 0.15, synthesized by liquid phase method.

3.1.2. Raman spectroscopy

The Raman spectra of the samples in the system $Na_{3+x}P_{1-x}Se_xS_4$, x = 0- 0.15, are shown in Figure 2 along with that of SeS_2. All spectra display the vibrational frequencies associated with the P–S bonds in PS_4^{3-}: the symmetric stretch at 411 cm^{-1}, the asymmetric stretch (doublet) at 550 cm^{-1}, and the in-phase and out-of-phase bending at 219 and 278 cm^{-1}, respectively [25]. The vibrational signals of SeS_2 are not detected until the Se content reaches x = 0.075. As the Se content increases beyond this value, traces of SeS_2-related peaks start to appear: one clearly visible at 471 cm^{-1}, and another at 263 cm^{-1} overlapping with the PS_4^{3-} peak at 274 cm^{-1} in the spectrum for x = 0.15. This observation is consistent with the XRD results and indicates that a Se content of x = 0.075 is the maximum limit at which Se can fully dissolve into the Na_3PS_4 lattice to form a single-phase material. The unreacted SeS_2 is not detected in the XRD patterns of the same samples, possibly due to its conversion to an amorphous state during agitation in the liquid reaction mixture.

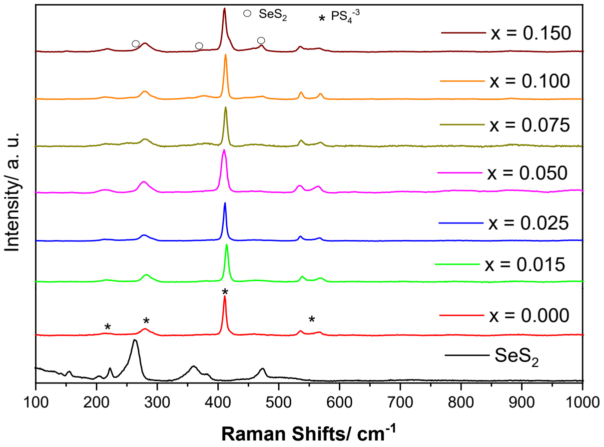

Figure 2. Raman spectra of $Na_{3+x}P_{1-x}Se_xS_4$ glass ceramics, x = 0 - 0.15, synthesized by liquid phase method.

3.1.3. Thermogravimetric analysis (TGA)

The TGA curves of selected precursor powders in the $Na_{3+x}P_{1-x}Se_xS_4$ system (Figure 3) display three distinct weight-loss events, highlighted by markers in the curve of the undoped sample. The first event occurs between 50 and 69 °C, immediately followed by the second, which ends around 105 °C. The third event begins at 200 °C and concludes at 266 °C. The initial weight loss is attributed to the release of physically adsorbed solvent molecules from the powder surface, while the second and third are ascribed to the removal of coordinated solvent molecules bound to the precursor components. These latter two weight-loss processes suggest the coexistence of two species, Na_3PS_4 and a residual intermediate, in the precursor. Each species likely forms distinct complexes with the solvent, which decompose at different temperatures during heating. As in the Li_3PS_4 system [26, 27], the formation of Na_3PS_4 is presumed to proceed via an intermediate, $Na_4P_2S_6$, which subsequently reacts with Na_2S to yield Na_3PS_4, following the mechanism:

$$2Na_2S + P_2S_5 \qquad Na_4P_2S_6 + S \qquad (1)$$

s

$$Na_2S + Na_4P_2S_6 + S \qquad 2Na_3PS_4 \qquad (2)$$

$$3Na_2S + P_2S_5 \qquad 2Na_3PS_4 \qquad (3)$$

Based on this mechanism, the intermediate $Na_4P_2S_6$ forms initially and subsequently transforms into Na_3PS_4 during the reaction. However, the conversion at ambient temperature proceeds rather slowly, leaving a considerable fraction of $Na_4P_2S_6$ unreacted and still coordinated with solvent molecules. During the synthesis process, the subsequent heating treatment releases the residual $Na_4P_2S_6$, which then reacts with the remaining Na_2S to yield Na_3PS_4 [28]. Hibi et al. [29] reported a characteristic Raman or infrared? band of $Na_4P_2S_6$ at ~380 cm^{-1} in ball-milled Na_3PS_4 precursor glass, which almost completely disappeared after heat treatment in the corresponding Na_3PS_4 glass–ceramic, confirming the consumption of the intermediate during the transformation. This stepwise conversion underscores the critical role of thermal treatment in achieving complete solvent removal and ensuring phase purity of the final Na_3PS_4 product. Consistent with these findings, Wan et al. [20] recommended a heating temperature of 270 °C to effectively remove solvent residues from Na_3PS_4 synthesised by the liquid phase method using ACN as a solvent.

While the Se-substituted samples exhibit a similar first weight-loss event as the undoped sample, clear differences emerge in the subsequent ones. The second weight-loss process becomes more pronounced and extended, whereas the third is significantly reduced and nearly undetectable. This behavior suggests that Se substitution improves the phase purity of the precursor, likely by decreasing the fraction of the intermediate phase. The effect may be attributed to an accelerated conversion of $Na_4P_2S_6$ into Na_3PS_4 in the presence of Se. Accordingly, the second and third weight-loss events can be assigned to the release of solvent molecules coordinated to Na_3PS_4 and $Na_4P_2S_6$, respectively.

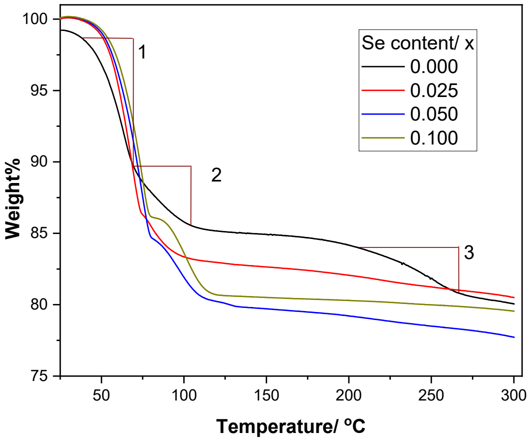

Figure 3. TGA curves of selected $Na_{3+x}P_{1-x}Se_xS_4$ samples precursors synthesised by liquid phase.

3.2. Ionic conductivity

The Nyquist impedance plots for the $Na_{3+x}P_{1-x}Se_xS_4$ samples (x = 0–0.15) are shown in Figure 4, with the corresponding conductivity values and activation energies summarized in Table 1. The ionic conductivity of the undoped sample is 0.0073 mS cm^{-1}, which falls within the range previously reported for this phase synthesized by liquid-phase methods using various solvents [12–14]. Upon selenium substitution, the conductivity increases and reaches a maximum at x = 0.05 (Table 1), after which it gradually decreases. A similar trend has been reported for As-substituted Na_3PS_4, where replacing P with As also enhanced ionic conductivity [30].

It has been reported that the main reason for the superionic conductivity of Na_3PS_4 is the structural defects that are formed during synthesis [31]. Therefore, enhancing these defects through the substitution with ions of different charges or sizes (iso/aliovalent ions) is expected to further enhance ionic conductivity. In this case, selenium, which is tetravalent Se(IV) when it replaces phosphorus (P(V)), has dual consequences. First, the requirement for charge neutrality leads to an increase in the number of sodium ions in the interstitial positions. The increase in interstitial sodium ions, serving as charge carriers, is expected to enhance the material's ionic conductivity. Furthermore, the substitution of smaller P^{+5} ions with larger Se^{+4} ions [24] induces lattice expansion and increases the free volume available for ion transfer [32]. Besides, the conductivity enhancement relative to the undoped sample is also consistent with the TGA results, which indicated that Se substitution improves the purity of the Na_3PS_4 precursor and consequently the final glass–ceramic product. The conductivity reaches a limiting value, likely due to saturation of interstitial sites with sodium ions, or due to the energetically unfavorable alloying, which leads to the precipitation of unreacted selenium sulfide as evidenced by the appearance of characteristic Raman bands of unreacted SeS_2 in samples with $x > 0.075$ (Figure 2).

The partial substitution of phosphorus with selenium in Na_3PS_4 alters the temperature required for the formation of the superionic glass–ceramic phase. As shown in Figure S2 (black pattern), heating the $Na_{3.025}P_{0.975}Se_{0.025}S_4$ precursor at 140 °C for 6 hours yields an XRD pattern that does not correspond to any crystalline phases in our database. Such patterns, frequently observed in thiosulfate precursors synthesized via liquid-phase methods, are typically attributed to the formation of solvent–precursor complexes [33]. Upon further heating at 150 °C for 2 hours, the XRD pattern changes to one characteristic of a crystalline cubic-tetragonal glass–ceramic (Figure S2m red pattern). This structural transformation coincides with the onset of superionic conduction, as confirmed by ionic conductivity measurements (Figure S3). Notably, the transition is not accompanied by any significant weight loss in the TGA curve (Figure 3), indicating that it does not arise from solvent release. Instead, it reflects the crystallization of Na_3PS_4, which is inherently superionic. As discussed earlier, Na_3PS_4 releases coordinated water at lower temperatures (~105 °C), whereas $Na_4P_2S_6$ retains coordinated solvent to much higher temperatures. Based on these observations, we attribute the featureless XRD patterns at 140 °C to solvent-coordinated $Na_4P_2S_6$, while the appearance of well-defined glass–ceramic peaks at 150 °C corresponds to the formation of Na_3PS_4, which is also responsible for the high ionic conductivity. The disappearance of the solvent-precursor complex's XRD pattern recorded at 150°C likely results from the overwhelming intensity of the glass ceramic pattern, rather than the complete loss of solvent. Additionally, we found that samples with higher selenium content transition to a superionic conductive crystalline phase at temperatures above 150°C, with the transition temperature increases as selenium content rises. For example, the sample x = 0.05 exhibited superionic conductivity phase at 180°C, while the sample x = 0.075 did so at 220°C. Consequently, we selected 270°C as the suitable temperature for heat treatment of the studied samples.

The temperature dependence of ionic conductivity follows the Arrhenius equation (see Figure S4), and the activation energies calculated by fitting the data to this equation are presented in Table 1. The activation energy of the undoped Na_3PS_4 sample is 0.367 eV, which is higher than that reported for ball-milled Na_3PS_4 [34], but lower [12] or comparable [13] to the values reported for the compound obtained by the liquid-phase method. Introducing selenium into the lattice slightly decreases the activation energy, which correlates with an increase in ionic conductivity up to a selenium content of x = 0.05. After this point, the activation energy continues to decrease, even as the ionic conductivity begins to decline. We hypothesize that increasing the selenium content further opens the structure, but the ionic conductivity begins to decrease due to an overwhelming number of sodium ions occupying the available interstitial sites.

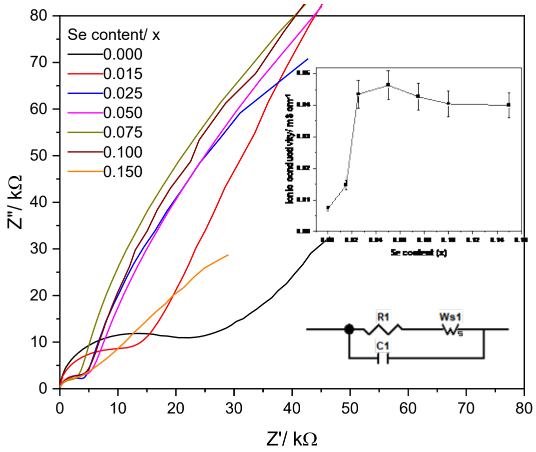

Figure 4: Impedance Nyquist plots of glass ceramics $Na_{3+x}P_{1-x}Se_xS_4$, x =0.000-0.150. The insets show the variation of the ionic conductivity with Se content, and the equivalent circuit to which the data was fitted.

Table 1: Lattice parameter *a*, Ionic conductivity at 298 K and activation energy of solid electrolytes $Na_{3+x}P_{1-x}Se_xS_4$, x = 0 - 0.15.

Se content/ x	**0.000**	**0.015**	**0.025**	**0.05**	**0.075**	**0.100**	**0.150**
σ/ mS cm^{-1}	0.007	0.015	0.044	0.046	0.043	0.040	0.040
E$_a$/ eV	0.367	0.337	0.301	0.332	0.326	0.288	0.285
a/ Å	7.0025 +/- 0.0004	7.0032 +/- 0.0003	7.0102+/- 0.0004	---	7.0168+/- 0.0002	----	7.0156+/- 0.0012

3.3. Electrochemical stability

The electrochemical stability of $Na_{3+x}P_{1-x}Se_xS_4$ was assessed via cyclic voltammetry (CV), selecting the sample $Na_{3.05}P_{0.95}Se_{0.05}S_4$ as a representative due to its high ionic conductivity. For this, a circular pellet (8 mm diameter and 0.8 mm thickness) was positioned between a stainless-steel disc and a 300 mm circular sheet of Na metal. The voltage was scanned between -0.5 and 4 V at 1 mV/s. The resulting cyclic voltammogram, shown in Figure 5, reveals peaks near 0 V (both positive and negative) due to sodium metal deposition and stripping on the stainless-steel surface under applied overpotentials. No additional peaks indicating solid electrolyte degradation were detected. Repeating the scan at a slower rate of 0.1 mV/s confirmed these results (Figure S5). These observations align with previous studies on ball-milled Na_3PS_4, supporting the electrochemical stability of the solid electrolyte within the 0-4 V range [6, 35].

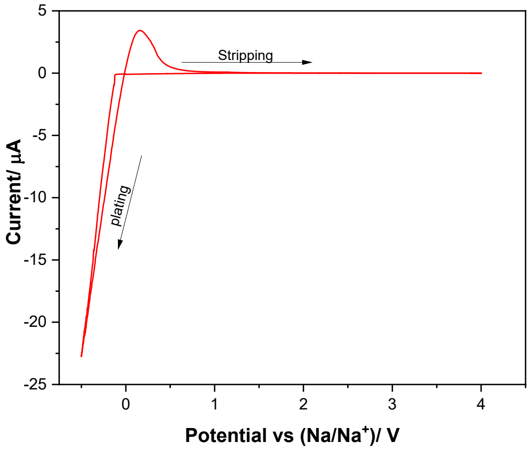

Figure 5. Cyclic voltammogram of the sample $Na_{3.05}P_{0.95}Se_{0.05}S_4$ in a half cell contains Na metal as reference electrode, stainless steel as working electrode and the sample as solid electrolyte separator. Voltage scan rate is 1 mV/s.

3.4. All sodium solid state battery

An all solid-state battery was assembled using $Na_{15}Sn_4$ as the negative electrode, $Na_{3.05}P_{0.95}Se_{0.05}S_4$ as the solid electrolyte, and a TiS_2-$Na_{3.05}P_{0.95}Se_{0.05}S_4$ (1:1) composite as the positive electrode. A second battery was assembled similarly, but with Na_3PS_4 synthesized by ball milling as a solid electrolyte for comparison. The liquid-phase-synthesized Na_3PS_4 was not selected as a benchmark in this study due to its relatively low ionic conductivity, which falls well below the threshold required for solid electrolyte applications. The two batteries were cycled over a voltage range of 1–2.8 V. The cycling and rate capability performances of both batteries are presented in Figure 6 (a-c). The charge-discharge curves show the typical two plateaus corresponding to the intercalation and conversion reactions of TiS_2 cathode material [36]. The batteries achieved comparable initial capacities of around 125 and 135 mAh g^{-1}, respectively, demonstrating the successful application of Se-substituted Na_3PS_4 in an all-solid-state battery. The ball-milled Na_3PS_4 displayed better rate capability, potentially due to its higher ionic conductivity. The initial capacities obtained in this work are close to those of batteries previously reported with Ball-milled solid electrolytes Na_3PS_4 [21, 37], Cl-doped Na_3PS_4 [16], and also comparable to those assembled using NASICON solid electrolytes [38].

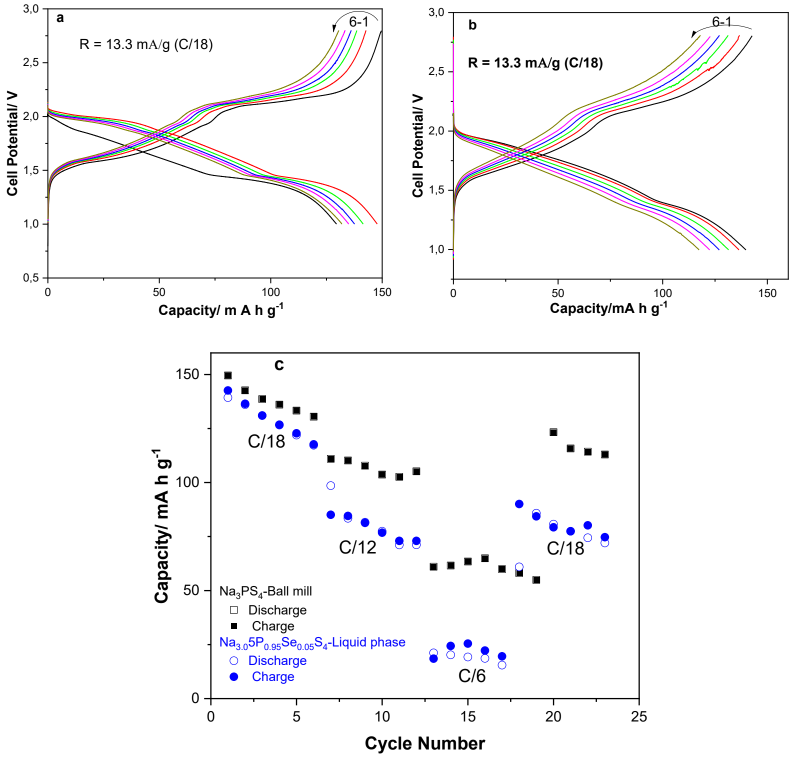

Figure 6: Cycling performance of ball milled Na_3PS_4 (a) and Liquid phase synthesised $Na_{3.05}P_{0.95}Se_{0.05}S_4$ (b), and rate capabilities of both samples (c).

Conclusion

The liquid-phase method was employed successfully for synthesizing solid electrolytes within the $Na_{3+x}P_{1-x}Se_xS_4$ system. The solid electrolyte with the highest ionic conductivity among these, $Na_{3.05}P_{0.95}Se_{0.05}S_4$, exhibited an ionic conductivity comparable to that of ball-milled Na_3PS_4. The increase in ionic conductivity in these samples is attributed to the extra free volume created by the larger tetravalent Se ion, as well as the higher concentration of interstitial sodium ions resulting from charge neutrality requirements. These solid electrolytes demonstrated electrochemical stability within the range of 0–4 V and achieved a battery performance comparable to that of ball-milled Na_3PS_4

Acknowledgment

The author (Mohammed Hassan) is grateful to Hasselt University and the Flemish government for funding his research stay through the SAR (Scientists at Risk) exchange program. The author Raheed Bolia thanks VLAIO Baekeland for the financial funding. We would like to thank Bart

Ruttens for conducting the XRD analysis, Gianfabio Mangione for the Raman analysis, Digvijay Ghogare for the TGA-FTIR analysis and Thomas Vranken for the technical support.

References

1. X. Yu, R. Chen, L. Gan, H. Li, L. Chen, Battery Safety: From Lithium-Ion to Solid-State Batteries, Engineering, 21(2023)9-14, https://doi.org/10.1016/j.eng.2022.06.022
2. S., Yang, Z., Wang, SB. et al. Sulfide-based composite solid electrolyte films for all-solid-state batteries. Commun Mater 5(2024)44. https://doi.org/10.1038/s43246-024-00482-8
3. A. Jannesar Niri, G. A. Poelzer, S. E. Zhang, J. Rosenkranz, M. Pettersson, and Y. Ghorbani, Sustainability challenges throughout the electric vehicle battery value chain, *Renewable and Sustainable Energy Reviews*, 191(2024)114176, https://doi.org/10.1016/j.rser.2023.114176
4. P. Greim, A. A. Solomon, and C. Breyer, Assessment of lithium criticality in the global energy transition and addressing policy gaps in transportation, *Nature Communications,*11, (1)(*2020)*,1–11, https://doi.org/10.1038/s41467-020-18402-y
5. Lifang Zhang, Yinghui Xia, Hao Yang, Sijie Xiao, Jinqiu Zhou, Yufeng Cao, Tao Qian, The current status of sodium metal anodes for improved sodium batteries and its future perspectives, *APL Mater*, 10(7)(2022) 070901, https://doi.org/10.1063/5.0097264
6. A. Hayashi, K. Noi, A. Sakuda, and M. Tatsumisago, Superionic glass-ceramic electrolytes for room-temperature rechargeable sodium batteries, *Nat Commun*, 3(2012) https://doi.org/10.1038/ncomms1843
7. S. Chen *et al.*, “Sulfide solid electrolytes for all-solid-state lithium batteries: Structure, conductivity, stability and application,” Sep. 01, 2018, *Elsevier B.V.* doi: 10.1016/j.ensm.2018.02.020.
8. J. Tang, J. Qiao, Z. Liu, X. Zhou, G. Yu, and J. Zhao, Mechanism characteristic analysis and soft measuring method review for ball mill load based on mechanical vibration and acoustic signals in the grinding process, *Miner Eng*, 128(2018)294–311, https://doi.org/10.1016/j.mineng.2018.09.006
9. J. Xu, L. Liu, N. Yao, F. Wu, H. Li, and L. Chen, Liquid-involved synthesis and processing of sulfide-based solid electrolytes, electrodes, and all-solid-state batteries, *Materials Today Nan,8*(2019) 100048, https://doi.org/10.1016/j.mtnano.2019.100048

10. Akira Miura, Nataly C. Rosero-Navarro, Atsushi Sakuda, Kiyoharu Tadanaga, Nguyen H. H. Phuc, Atsunori Matsuda, Nobuya Machida, Akitoshi Hayashi, Masahiro Tatsumisago, Liquid-phase syntheses of sulfide electrolytes for all-solid-state lithium battery, *Nat. Rev. Chem., 3*(2019)189–198, https://doi.org/10.1038/s41570-019-0078-2

11. Masakuni Takahashi, Seunghoon Yang, Kentaro Yamamoto, Koji Ohara, Nguyen Huu Huy Phuc, Toshiki Watanabe, Tomoki Uchiyama, Atsushi Sakuda, Akitoshi Hayashi, Masahiro Tatsumisago, Hiroyuki Muto, Atsunori Matsuda, Yoshiharu Uchimoto, Improvement of lithium ionic conductivity of Li_3PS_4 through suppression of crystallization using low-boiling-point solvent in liquid-phase synthesis, *Solid State Ion*, 361, (2021) 115568, https://doi.org/10.1016/j.ssi.2021.115568.

12. M. Atsunori, G. Hirotada, and N. H. H. Phuc, "Preparation of cubic Na3PS4 by liquid-phase shaking in methyl acetate medium," *Heliyon*, 5(11)(2019)115568, https://doi.org/10.1016/j.ssi.2021.115568

13. M. Uematsu, S. Yubuchi, K. Noi, A. Sakuda, A. Hayashi, and M. Tatsumisago, Preparation of Na_3PS_4 electrolyte by liquid-phase process using ether, *Solid State Ion*, 320(2018)33–37, https://doi.org/10.1016/j.ssi.2017.12.021

14. S. Yubuchi, A. Hayashi, and M. Tatsumisago, Sodium-ion conducting Na_3PS_4 electrolyte synthesized via a liquid-phase process using N-methylformamide, *Chem Lett*, 44(7)(2015)884–886, https://doi.org/10.1246/cl.150195

15. L. Bekaert, S. Akatsuka, N. Tanibata, F. De Proft, A. Hubin, M. H. Mamme, M. Nakayama, Increasing the Sodium Metal Electrode Compatibility with the Na_3PS_4 Solid-State Electrolyte through Heteroatom Substitution, *ChemSusChem*,16(2023)e202300676, https://doi.org/10.1002/cssc.202300676

16. Iek-Heng Chu, Christopher S. Kompella, Han Nguyen, Zhuoying Zhu, Sunny Hy, Zhi Deng, Ying S. Meng, Shyue P. Ong, Room-Temperature All-solid-state Rechargeable Sodium-ion Batteries with a Cl-doped Na_3PS_4 Superionic Conductor," *Scientific Reports* 6(1)(2016)1–10, https://doi.org/10.1038/srep33733

17. N. Tanibata, K. Noi, A. Hayashi, and M. Tatsumisago, Preparation and characterization of highly sodium ion conducting Na_3PS_4-Na_4SiS_4 solid electrolytes," *RSC Adv*, 4(33)(2014)17120–17123, https://doi.org/10.1039/C4RA00996G

18. K. Hogrefe, J. Königsreiter, A. Bernroitner, B. Gadermaier, S. E. Ashbrook, and H. M. R. Wilkening, Length-Scale-Dependent Ion Dynamics in Ca-Doped Na_3PS_4," *Chemistry of Materials*, 36(2)(2024)980–993, https://doi.org/10.1021/acs.chemmater.3c02874

19. F. Tsuji, A. Nasu, A. Sakuda, M. Tatsumisago, and A. Hayashi, Mechanochemical synthesis and characterization of $Na_{3-x}P_{1-x}W_xS_4$ solid electrolytes, *J Power Sources*, 506(2021)230100, https://doi.org/10.1016/j.jpowsour.2021.230100

20. Hongli Wan, Jean P. Mwizerwa, Xingguo Qi, Xiaoxiong Xu, Hong Li, Qiang Zhang, Liangting Cai, Yong-Sheng Hu, Xiayin Yao, Nanoscaled Na_3PS_4 Solid Electrolyte for All-Solid-State FeS_2/Na Batteries with Ultrahigh Initial Coulombic Efficiency of 95% and Excellent Cyclic Performances, *ACS Appl Mater Interfaces*,10(15)(2018)12300–12304, https://doi.org/10.1021/acsami.8b01805

21. N. Tanibata, T. Matsuyama, A. Hayashi, and M. Tatsumisago, All-solid-state sodium batteries using amorphous TiS_3 electrode with high capacity, *J Power Sources*, 275(2015)284–287, https://doi.org/10.1016/j.jpowsour.2014.10.193

22. Han Nguyen, Abhik Banerjee, Xuefeng Wang, Darren Tan, Erik A. Wu, Jean-Marie Doux, Ryan Stephens, Guy Verbist, Ying Shirley Meng, Single-step synthesis of highly conductive Na3PS4 solid electrolyte for sodium all solid-state batteries, *J Power Sources*, 435(2019)126623, https://doi.org/10.1016/j.jpowsour.2019.05.031

23. T. Krauskopf, S. P. Culver, and W. G. Zeier, "Local Tetragonal Structure of the Cubic Superionic Conductor Na_3PS_4, *Inorg Chem*, 57(8)(2018)4739–4744, https://doi.org/10.1021/acs.inorgchem.8b00458

24. E. J. W. Whittaker and R. Muntus, Ionic radii for use in geochemistry, *Geochim Cosmochim Acta*, 34(9)(1970)945–956, https://doi.org/10.1016/0016-7037(70)90077-3

25. Theodosios Famprikis, Houssny Bouyanfif, Pieremanuele Canepa, Mohamed Zbiri, James A. Dawson, Emmanuelle Suard, François Fauth,Helen Y. Playford, Damien Dambournet, Olaf J. Borkiewicz, Matthieu Courty, Oliver Clemens Jean-Noël Chotard, M. Saiful Islam, ChristianMasquelier, Insights into the Rich Polymorphism of the Na^+ Ion Conductor Na_3PS_4 from the Perspective of Variable-Temperature Diffraction and Spectroscopy, *Chemistry of Materials*,33(14)(2021)5652–5667, https://doi.org/10.1021/acs.chemmater.1c01113

26. R. Poirier, D. Pasquier, A. Lambert, M. Corral Valero, D. Uzio, and C. Garnero, Solvent Key Parameters for the Wet Chemical Synthesis of the Li3PS4 Solid Electrolyte, *Journal of Physical Chemistry C*, 128(28)(2024)128–11477, https://doi.org/10.1021/acs.jpcc.4c01598

27. F. M. Delnick, G. Yang, E. C. Self, H. M. Meyer, and J. Nanda, Investigation of complex intermediates in solvent-mediated synthesis of thiophosphate solid-state electrolytes, *Journal of Physical Chemistry C*, (124)(50)(2020)27396–27402, https://doi.org/10.1021/acs.jpcc.0c08761

28. Kentaro Yamamoto, Seunghoon Yang, Masakuni Takahashi, Koji Ohara, Tomoki Uchiyama, Toshiki Watanabe, Atsushi Sakuda, Akitoshi Hayashi, Masahiro Tatsumisago, Hiroyuki Muto, Atsunori Matsuda, and Yoshiharu Uchimoto, High Ionic Conductivity of Liquid-Phase-Synthesized Li_3PS_4 Solid Electrolyte, Comparable to That Obtained via Ball Milling, *ACS Appl Energy Mater*, 4(3)(2021)2275–2281, https://doi.org/10.1021/acsaem.0c02771

29. Yoshiaki Hibi, Naoto Tanibata, Akitoshi Hayashi, Masahiro Tatsumisago, Preparation of sodium ion conducting Na3PS4–NaI glasses by a mechanochemical technique, Solid State Ionics, 270(2015) 6-9, https://doi.org/10.1016/j.ssi.2014.11.024.

30. Zhaoxin Yu, Shun-Li Shang, Joo-Hwan Seo, Daiwei Wang, Xiangyi Luo,Qingquan Huang, ShuruChen, Jun Lu, Xiaolin Li, Zi-Kui Liu, Donghai Wang, Exceptionally High Ionic Conductivity in $Na_3P_{0.62}As_{0.38}S_4$ with Improved Moisture Stability for Solid-State Sodium-Ion Batteries, *Advanced Materials*, 29(16)(2017), https://doi.org/10.1002/adma.201605561

31. Z. Zhu, I. H. Chu, Z. Deng, and S. P. Ong, Role of Na^+ Interstitials and Dopants in Enhancing the Na+ Conductivity of the Cubic Na_3PS_4 Superionic Conductor, *Chemistry of Materials*, 27(24)(2015)8318–8325, https://doi.org/10.1021/acs.chemmater.5b03656

32. Zhenming Xu, Can large lattice volume always facilitate ion diffusion in solids?, Energy Storage Materials, 69(2024)103433, https://doi.org/10.1016/j.ensm.2024.103433

33. Frank M. Delnick, Guang Yang, Ethan C. Self, Harry M. Meyer III, and Jagjit Nanda, Investigation of Complex Intermediates in Solvent-Mediated Synthesis of Thiophosphate Solid-State Electrolytes, *The Journal of Physical Chemistry C*, 124 (50)(2020)27396-27402, DOI: 10.1021/acs.jpcc.0c08761

34. A. Hayashi, K. Noi, N. Tanibata, M. Nagao, and M. Tatsumisago, High sodium ion conductivity of glass-ceramic electrolytes with cubic Na_3PS_4, *J Power Sources*, 258(2014)420–423, https://doi.org/10.1016/j.jpowsour.2014.02.054

35. Xiaoyan Xu, Yuanyuan Li, Jun Cheng, Guangmei Hou, Xiangkun Nie, Qing Ai, Linna Dai, Jinkui Feng, Lijie Ci, Composite solid electrolyte of Na_3PS_4-PEO for all-solid-state SnS_2/Na batteries with excellent interfacial compatibility between electrolyte and Na metal, *Journal of Energy Chemistry*, 41(2020)73–78, https://doi.org/10.1016/j.jechem.2019.05.003

36. Hongwei Tao, Min Zhou, Ruxing Wang, Kangli Wang, Shijie Cheng, Kai Jiang, TiS2 as an Advanced Conversion Electrode for Sodium-Ion Batteries with Ultra-High Capacity and Long-Cycle Life, *Adv. Sci.,* 5(2018)1801021, https://doi.org/10.1002/advs.201801021

37. M. Mwemezi, W. B. Park, and A. B. Ikhe, Improvement of interfacial stability between Na metal and Na_3PS_4 family solid electrolyte for all-solid-state sodium metal batteries, *Electrochim Acta*, 480(2024)143919, https://doi.org/10.1016/j.electacta.2024.143919

38. Haoqing Tian, Shan Liu, Lijun Deng, Ling Wang, Lei Dai, New-type Hf-based NASICON electrolyte for solid-state Na-ion batteries with superior long-cycling stability and rate capability, Energy Storage Materials, 39(2021)232-238, https://doi.org/10.1016/j.ensm.2021.04.026

Supplementary material

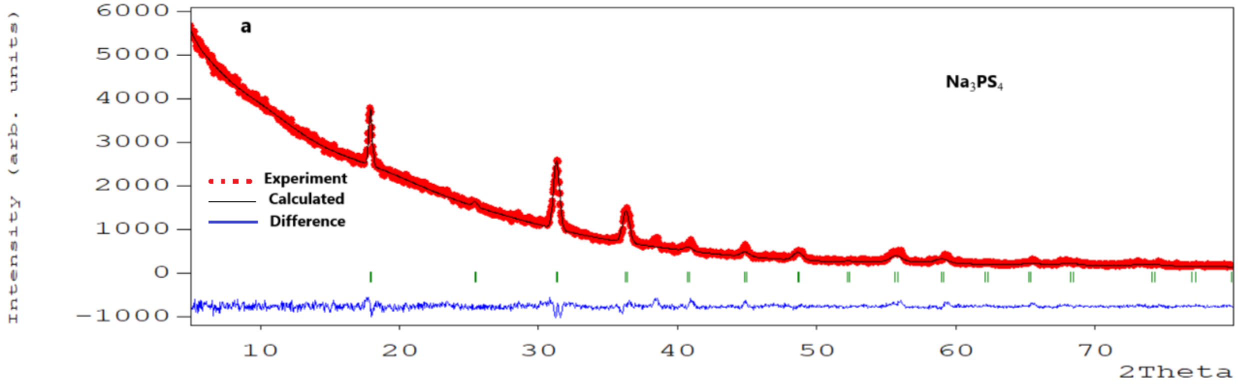

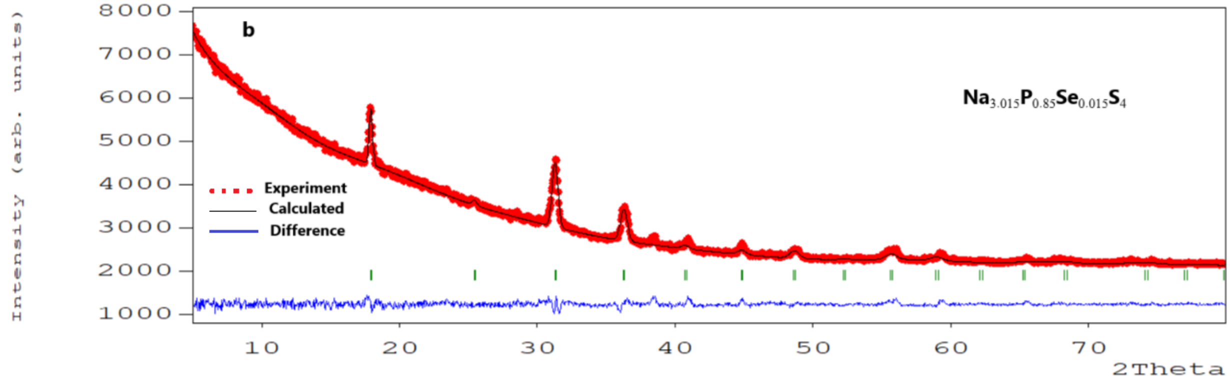

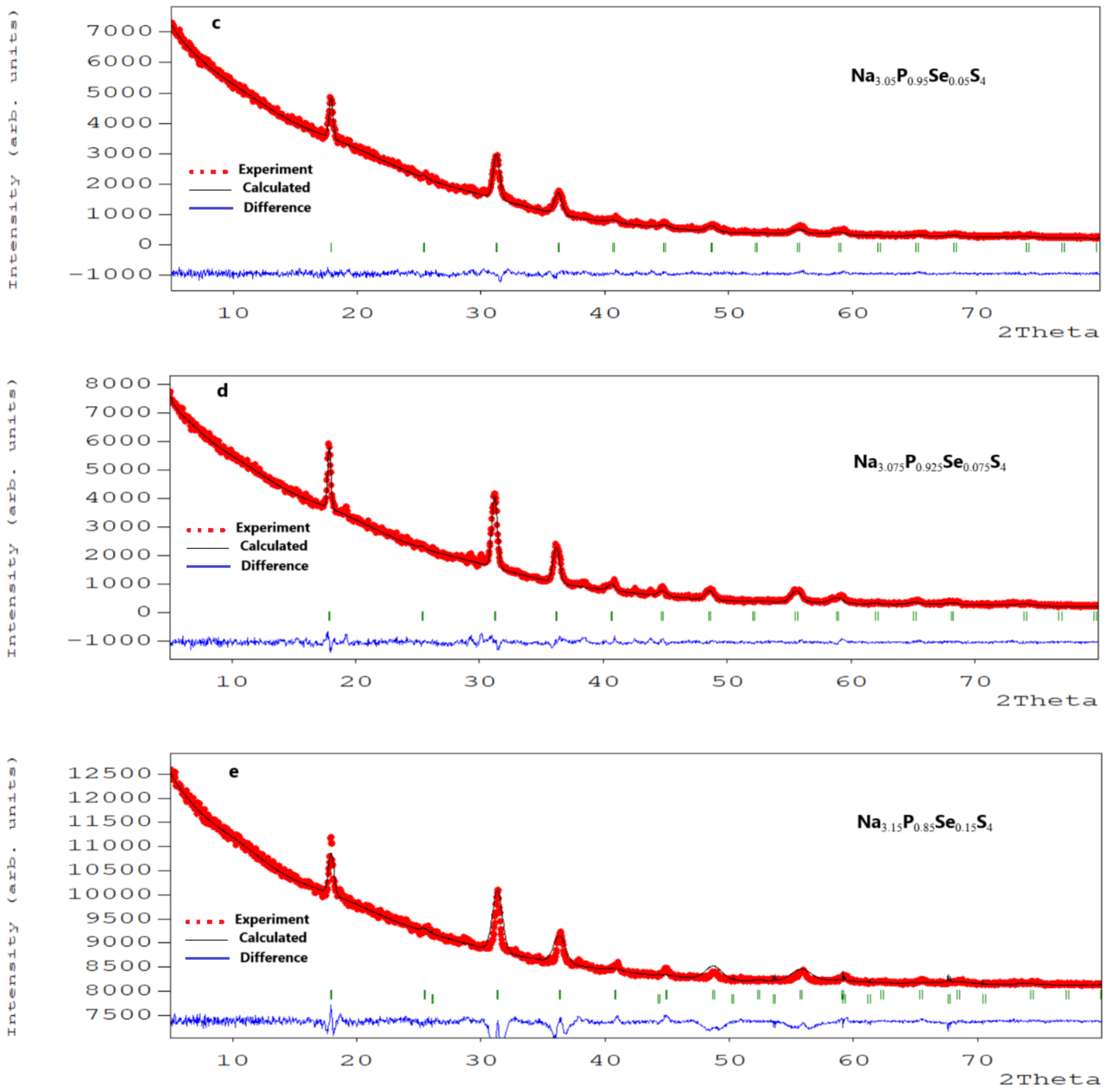

Figure S1(a-e): Rietveld refinement profiles of the XRD patterns for samples $Na_{3+x}P_{1-x}Se_xS_4$.

Table S1. Calculated Lattice parameter (*a*) of samples $Na_{3+x}P_{1-x}Se_xS_4$.

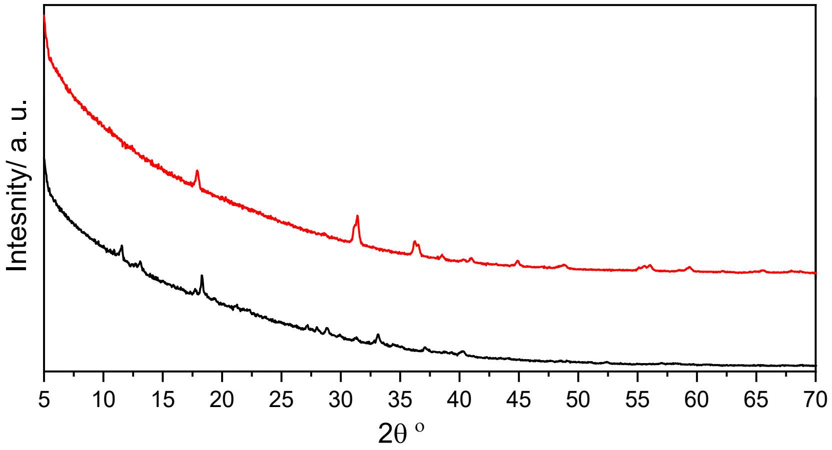

Figure S2: XRD patterns of $Na_{3.025}P_{0.975}Se_{.025}S_4$ heat treated at 140°C for 6h (black), and 150°C for 2h (red).

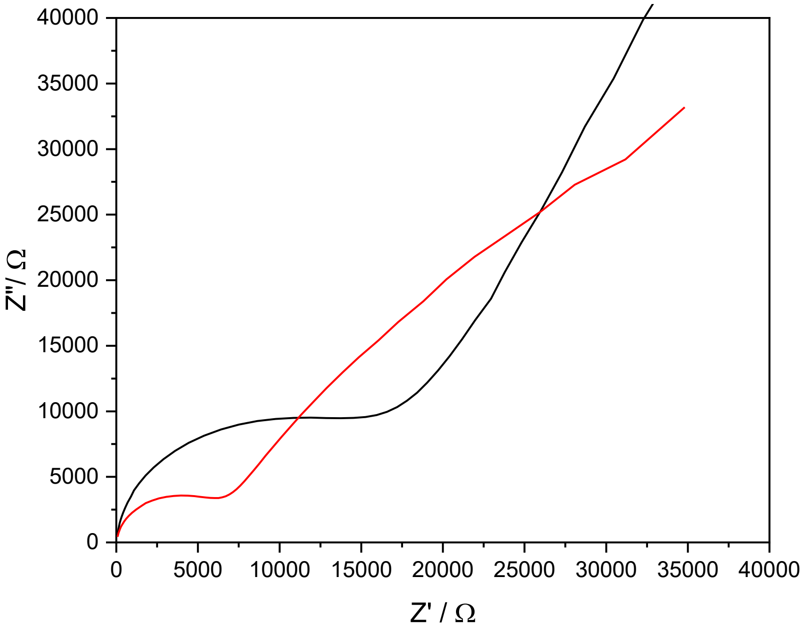

Figure S3: Nyquist impedance plots of $Na_{3.025}P_{0.975}Se_{0.025}S_4$ sample at 140 (black) and 150 (red).

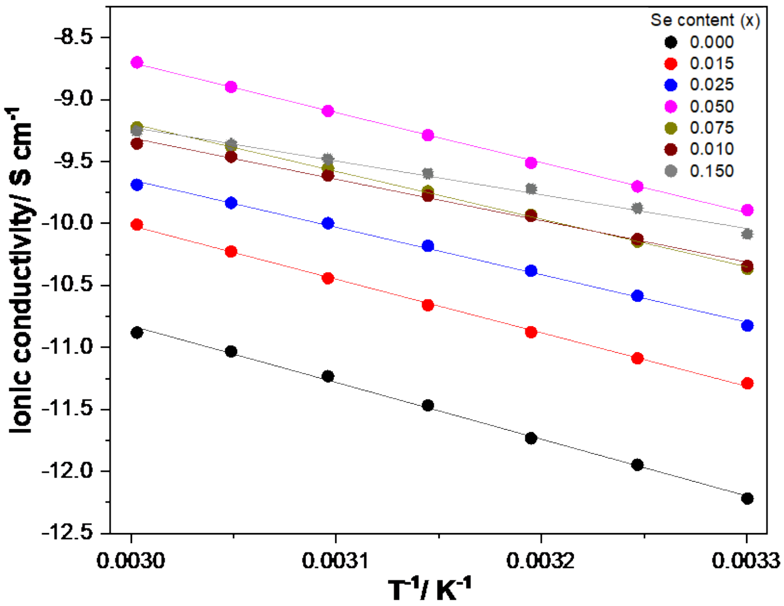

Figure S4: Temperature dependence of ionic conductivity of the system $Na_{3+x}P_{1-x}Se_xS_4$, x = 0, -0.15.

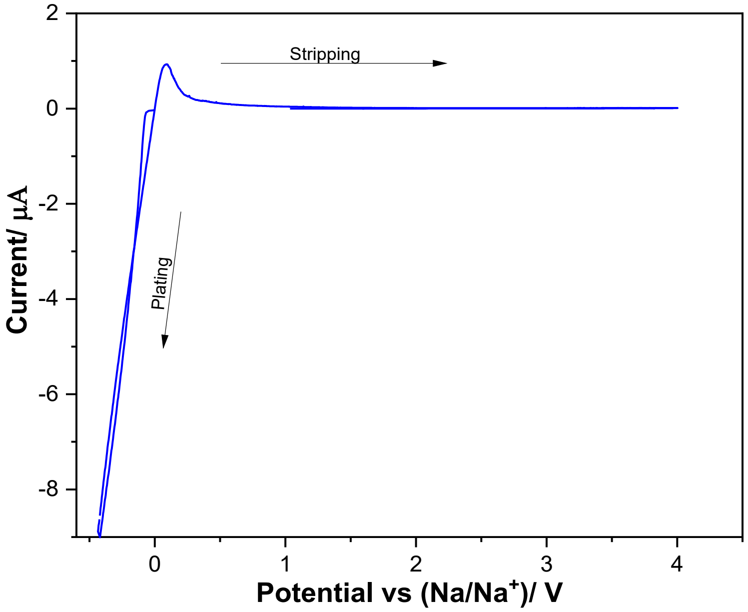

Figure S5. Cyclic voltammogram of the sample $Na_{3.05}P_{0.95}Se_{0.05}S_4$ in a half cell contains Na metal as reference electrode, stainless steel as working electrode and the sample as solid electrolyte separator. Voltage scan rate is 0.1 mV/s.